



Improved representation of the contemporary Greenland ice sheet firn layer by IMAU-FDM v1.2G

Max Brils¹, Peter Kuipers Munneke¹, Willem Jan van de Berg¹, and Michiel van den Broeke¹

¹Institute for Marine and Atmospheric Research, Utrecht University, Utrecht, the Netherlands

Correspondence: Max Brils (m.brils@uu.nl)

Abstract.

The firn layer that covers 90% of the Greenland ice sheet (GrIS) plays an important role in determining the response of the ice sheet to climate change. Meltwater can percolate into the firn layer and refreeze at greater depths, thereby temporarily preventing mass loss. However, as global warming leads to increasing surface melt, more surface melt may refreeze in the firn layer, thereby reducing the capacity to buffer subsequent episodes of melt. This can lead to a tipping point in meltwater runoff. It is therefore important to study the evolution of the Greenland firn layer in the past, present and future. In this study, we present the latest version of our firn model, IMAU-FDM (Firn Densification Model) v1.2G, with an application to the GrIS. We improved the density of freshly fallen snow, the dry-snow densification rate and the firn's thermal conductivity using recently published parameterizations and by calibrating to an extended set of observations of firn density, temperature and liquid water content at the GrIS. Overall, the updated model settings lead to higher firn air content and higher 10 m firn temperatures, owing to a lower density near the surface. The effect of the new model settings on the surface elevation change is investigated through three case studies located at Summit, KAN-U and FA-13. Most notably, the updated model shows greater inter- and intra-annual variability in elevation and an increased sensitivity to climate forcing.

1 Introduction

Firn, the layer of compressed snow that represents the transitional stage between seasonal snow and ice in the accumulation zone of glaciers, strongly influences the climate response of mountain glaciers, ice caps and ice sheets. Pore space between snow grains that make up the firn layer enable meltwater to percolate into the firn layer, and refreeze – if the firn temperatures is below freezing. This prevents runoff. It has been demonstrated that refreezing is a critical process for many ice caps to survive, e.g. in the Canadian Arctic. On these ice caps, summer melt consistently exceeds annual snowfall, and refreezing is required to maintain a near-zero mass balance (Noël et al. (2018a)). As melt rates increase further in response to global warming, firn pore space is increasingly taken up by refrozen meltwater, degrading the efficiency of the refreezing process until at some point it collapses. This is happening to Greenland's marginal ice caps since the mid 1990s, accelerating mass loss and initiating their irreversible demise in the coming centuries (Noël et al. (2017)).

This saturation tipping point is not yet reached for the Greenland ice sheet (GrIS). The GrIS has a much more extensive firn layer ($\sim 1.4 \cdot 10^6 \text{ m}^2$), covering about 80% of the total area of the GrIS, which is higher in elevation (on average 2100



m above sea level (a.s.l.) and hence more porous and colder than firn on other Arctic ice caps (Noël et al. (2020)). With a depth of up to 80 m (Kuipers Munneke et al. (2015a)), Vandecrux et al. (2019b) estimated that the GrIS firn layer contains a total of $26800 \pm 1840 \text{ km}^3$ of air. This is equivalent to more than 60 times the total annual (1961-1990 average) volume of GrIS meltwater production (Van den Broeke et al. (2016)), although this reduces to a factor of $\sim 1-4$ if only pore space in the percolation zone is considered (Harper et al. (2012b)). Model estimates show that for the same period, no less than 44% of the meltwater produced at the surface of the GrIS refroze in the firn layer (Van den Broeke et al. (2016); Mouginit et al. (2019)).

Surface melt is also increasing in the GrIS accumulation zone, with the extreme melt summers of 2012 and 2019 as vivid examples (Nghiem et al. (2012); Sasgen et al. (2020)). These high-melt summers also led to peaks in refreezing, warming and densification of the firn layer (Steger et al. (2017a)). In some places, 1-2 m thick ice slabs are formed that prevent meltwater from reaching the pore space below (Machguth et al. (2016); MacFerrin et al. (2019)).

Diagnosing the current state of the GrIS firn layer, and predicting its future, is evidently important. Firn density models can be used to interpolate between the relatively sparse observations from firn cores and snow pits (Kuipers Munneke et al. (2015a); Vandecrux et al. (2019b)). Another important application of modelled firn depth changes is the conversion of remotely sensed elevation (volume) changes to mass changes (Zwally et al. (2015); Wouters et al. (2015); Shepherd et al. (2020)). Some (regional) climate models are interactively coupled to a snow/firn model, but these often use simplified initialization, parametrizations and/or reduced vertical resolution for computational efficiency. The main advantage of using a dedicated, offline firn densification model is the lower computational cost, which enables the use of higher vertical resolution, a proper initialization of the firn layer, and extensive sensitivity testing (Lundin et al. (2017); Stevens et al. (2020); Vandecrux et al. (2020)). The drawback of using an offline firn model is that it must be forced unidirectionally with observed and/or modelled surface temperature and surface mass fluxes (snow, rain, sublimation, drifting snow erosion).

In this study we present an updated version of the firn densification model of the Institute for Marine and Atmospheric research Utrecht (IMAU-FDM v1.2G, henceforth IMAU-FDM) applied to the GrIS, forced at the upper boundary by the latest three-hourly output of the polar version of the Regional Atmospheric Climate Model (RACMO2, Noël et al. (2018b)). It supersedes the previous model version presented by Kuipers Munneke et al. (2015a) and Ligtenberg et al. (2018).

We use recently published parametrizations and previously existing and newly obtained observations of firn density, temperature and liquid water content from the GrIS to calibrate model parametrizations for surface (fresh snow) density, dry snow densification rate, thermal conductivity, and meltwater percolation. The updated model is subsequently used to perform case studies of contemporary firn depth variability in three climatologically distinct locations of the GrIS accumulation zone: (1) the dry and cold interior, (2) the relatively low-accumulation western percolation zone, and (3) the high-accumulation south-eastern percolation zone.

This paper is organized as follows. In Sect. 2 we describe a more extended set of observations, both in time and space, that allows for new parametrizations and improved calibration of IMAU-FDM for the GrIS. In Sect. 2.2 we show how the altered densification and heat conduction expressions (in that order) resulted in an overall improved representation of GrIS firn density, temperature and liquid water content. The three case studies are then presented in Sect. 4, followed in Sect. 5 by a summary and outlook.



2 Methods

2.1 Observations

IMAU-FDM output is evaluated using previously available and newly obtained profiles of firn density, temperature and liquid water content from the GrIS accumulation zone. The observations are from 128 different locations to ensure that the various ice facies and climate zones of the GrIS are well represented (Fig. 1). Vertical profiles of observed firn density from ice cores vary in depth from 9.6 to 150.8 m and have been drilled between 1952 and 2018 in the framework of the Program for Arctic Regional Climate Assessment (PARCA; McConnell et al. (2000); Mosley-Thompson et al. (2001); Hanna et al. (2006); Banta and McConnell (2007)), the Arctic Circle Traverses (ACT, Box et al. (2013)) and the EGIG line (Harper et al. (2012b)), Das 1 and Das 2 (e.g. from Hanna et al. (2006)) and several other cores were retrieved from the SUMup database (SURface Mass balance and snow depth on sea ice working group), (Koenig et al. (2013); Koenig and Montgomery (2019)).

Temperature observations include profiles ranging in depth between 4 and 14 m obtained by Harper et al. (2012b) along a transect in the western GrIS and at the NEEM deep ice core drilling site (Orsi et al. (2017)). Additional firn temperature observations are from Summit, Dye-2 (Vandecrux et al. (2019a), KAN-U (Charalampidis et al. (2015)) and FA-13 (Koenig et al. (2014)). An additional 14 observations of 10 m firn temperatures are from Polashenski et al. (2014).

For observations of liquid water in firn, we use observations from Dye-2 (Heilig et al. (2018)), obtained using an upward-looking ground-penetrating radar (upGPR), which was installed and operated in the summer of 2016. The upGPR was buried ~ 4.5 m under the snow, and was capable of measuring the liquid water percolation depth, content as well as the changing distance between the instrument and the snow surface. Although the data do not cover a wide spatial (single location) or temporal range (1 May-16 October 2016), they are unique and moreover have high temporal and vertical resolution, making them very valuable for firn model evaluation (Vandecrux et al. (2020)), but also to evaluate melt intensity and timing in the forcing time series.

2.2 IMAU-FDM

For this work we use the offline IMAU-FDM, a semi-empirical firn densification model that simulates the time evolution of firn density, temperature, liquid water content and changes in surface elevation owing to variability of firn depth. The model has been compared extensively to, and calibrated with observations of firn density and temperature from the ice sheets of Greenland and Antarctica (Ligtenberg et al. (2011); Kuipers Munneke et al. (2015a); Ligtenberg et al. (2018)). IMAU-FDM is forced by three-hourly output of the polar version of the Regional Atmospheric Climate Model (RACMO2.3p2) (Noël et al. (2019)). Over glaciated grid cells, the RACMO2 subsurface model uses approximately the same expressions as IMAU-FDM, but with a lower vertical resolution (max. 150 vs. 3000 layers) and less comprehensive initialization to save computation time. In the current version of IMAU-FDM we do not consider the subsurface penetration of shortwave radiation (Van Dalum et al. (2020)). For both the ice sheets of Greenland and Antarctica, the performance of IMAU-FDM has been comparable to the more physically-based SNOWPACK model (Steger et al. (2017b); Van Wessem et al. (2021); Keenan et al. (2021)). In the following

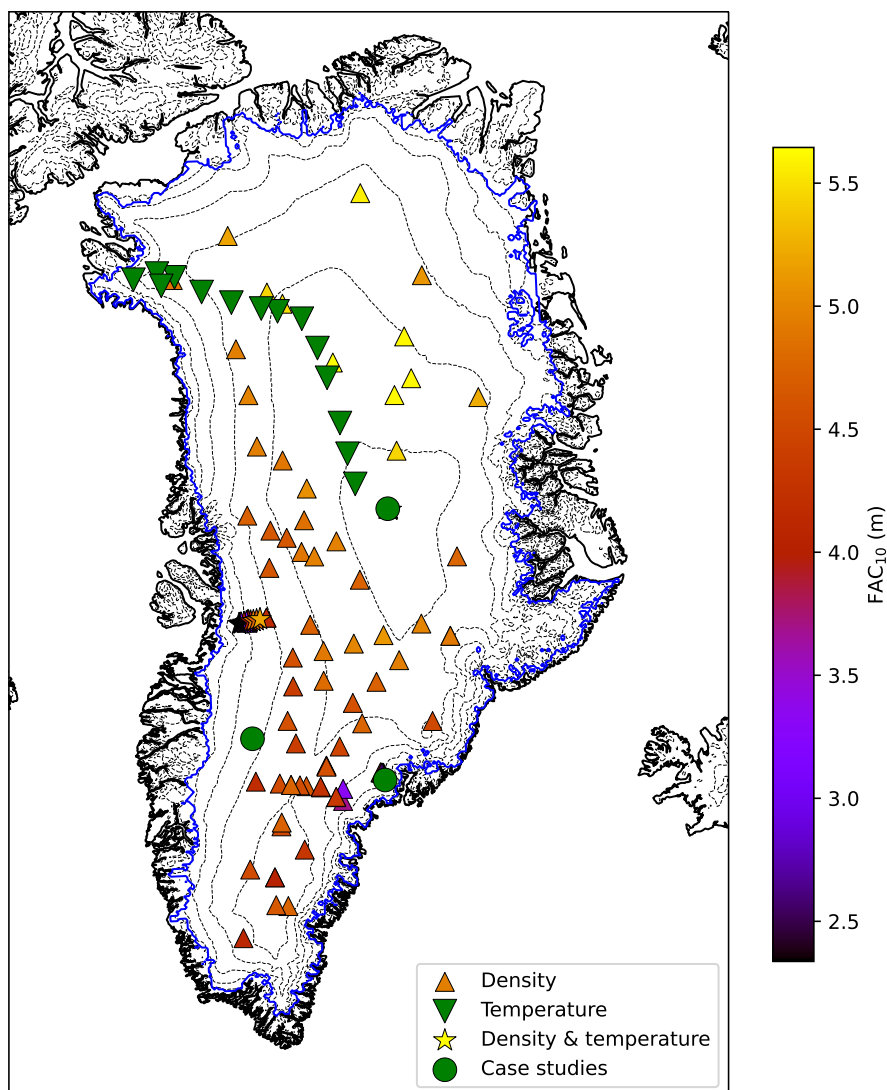


Figure 1. Locations of observed density (upward triangle), 10 m temperature (downward triangle), both (stars). The colour of the upward triangles and stars indicate the measured firm air content for the first 10 m of snow at that location (FAC₁₀). The three purple circles indicate the case studies discussed in Sect. 4. Dashed lines represent 500 m elevation contours, the blue solid line the contiguous ice sheet margin.

subsections, we briefly describe how the main processes are currently represented in IMAU-FDM, and what improvements have been implemented compared to the previous model version.



95 2.2.1 Fresh snow density

An important boundary condition for the model is the density of freshly fallen snow, ρ_0 . When determined from field observations, fresh snow density is often assumed equal to the near-surface density, loosely defined as the average density of the top 0.5 m of dry snow. As density is highly variable near the surface, the exact chosen depth is critical for the outcome, which hampers a robust comparison between datasets (Fausto et al. (2018)). In firn models, fresh snow density is commonly parameterized as a function of meteorological variables such as temperature and wind speed at the time of deposition, or, when these are not available, using annual average values instead (Keenan et al. (2021)). Several studies have addressed the parametrization of ρ_0 on the GrIS (Kuipers Munneke et al. (2015a); Fausto et al. (2018)). Assuming a linear dependence of the density on mean annual surface temperature T_s , this parametrization takes on the following form:

$$\rho_0 = A + B \cdot T_s \quad (1)$$

105 With A and B being fitting constants and T_s in $^{\circ}\text{C}$. In previous studies where IMAU-FDM was applied to the GrIS, $A = 481 \text{ kg m}^{-3}$ and $B = 4.834 \text{ kg m}^{-1}\text{K}^{-1}$ have been used (Kuipers Munneke et al. (2015a); Ligtenberg et al. (2018)) based on observations using the top 0.2 m average density from no-melt locations to approximate the surface value.

In the updated model, a new parameterization for fresh snow density (Fausto et al. (2018)) was adopted. In contrast to previous studies, which typically use the first $\sim 0.5 - 1.0$ m of snow, Fausto et al. (2018) used only the upper 0.1 m of snow to define surface density at 200 locations and found:

$$\rho_0 = 362.1 + 2.78 \cdot T_a \quad (2)$$

with T_a the annual mean near-surface (usually 2 m) air temperature in $^{\circ}\text{C}$.

Previously, the climatological mean 2 m air temperature has been used in IMAU-FDM (Kuipers Munneke et al. (2015b)), or an instantaneous value (Ligtenberg et al. (2018)). Using a climatological mean value suppresses the year-to-year variability in snow density. This is undesirable, especially because the model will also be used future scenarios, in which long term trends in temperature may have an effect. On the other hand, using instantaneous temperature values may introduce an excessive variability which, in reality, is smoothed by the effects of the snow being subjected to settling by wind and metamorphosis through numerous, daily warming and cooling cycles. As a trade-off, T_a in the updated model is calculated as the average 2 m air temperature of the year preceding the snowfall.

120 Fig. 2 shows the surface density (2010-2016) using three different approaches at site Das2 in Southeast Greenland. Clearly, temporal variations are much larger when an instantaneous T is used. Furthermore, the expression by Fausto et al. (2018) results in a lower surface density overall than Kuipers Munneke et al. (2015b). In subsequent sections, we refer to Ligtenberg et al. (2018) as the “old settings”.

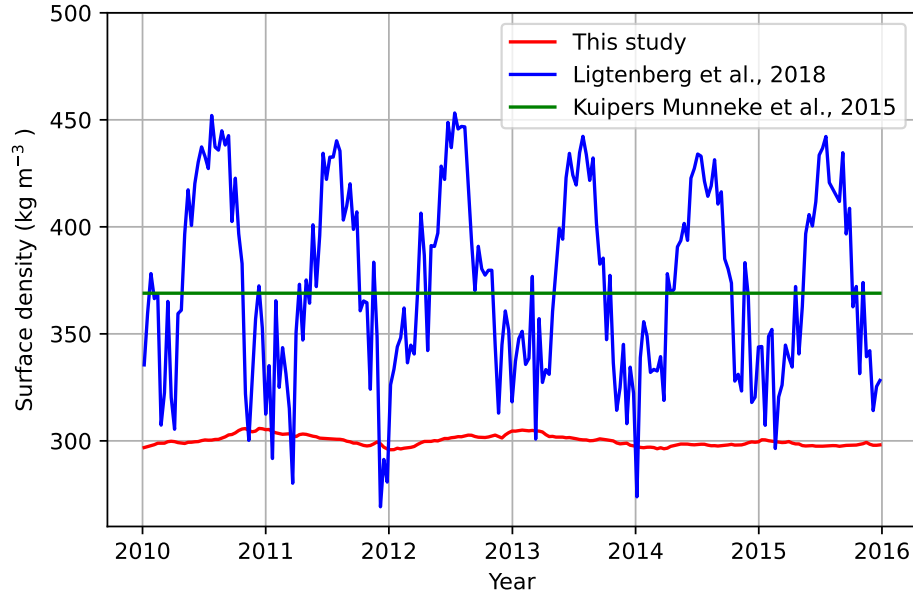


Figure 2. Daily averages of Das2 (southeast Greenland, see Fig. 1) surface density (2010-2016) using three different parametrizations.

2.2.2 Dry snow densification rate

125 IMAU-FDM is a 1D, vertical Lagrangian model. When new snow accumulates at the surface (model top), the model layers are buried deeper and tracked during their downward motion. At every time step, each layer is compacted under the influence of the pressure exerted by the mass of snow/firn above it. However, in IMAU-FDM the densification rate $\frac{d\rho}{dt}$ is not directly related to the overburden pressure, but rather follows a semi-empirical, temperature-dependent equation based on Arthern et al. (2010):

$$130 \quad \frac{d\rho}{dt} = C \dot{b} g (\rho_i - \rho) e^{-\frac{E_c}{RT} + \frac{E_g}{RT_{ave}}} \quad (3)$$

where \dot{b} is the annual average accumulation rate (mm w.e. per year) over the spinup-period (1960-1979), $\rho_i = 917 \text{ kg m}^{-3}$ is the density of glacial ice, g , E_c , E_g and R are constants, and T is the instantaneous layer temperature in Kelvin. The average annual accumulation rate \dot{b} is provided by RACMO2 as the amount of total precipitation minus sublimation and drifting snow erosion. Different values of C above and below $\rho = 550 \text{ kg m}^{-3}$ represent a shift in the dominant densification mechanism (Cuffey and Paterson (2011)). For $\rho < 550 \text{ kg m}^{-3}$, the densification of the firn is dominated by the settling and sliding of grains. For $\rho \geq 550 \text{ kg m}^{-3}$ recrystallisation, deformation and sublimation become dominant and the densification rate is lower, which is reflected in a lower value for C .

Compared to observations of the depth of the 550 and 830 kg m^{-3} density levels, a structural bias is found in Eq. 3, that in previous studies turned out to depend on the annual average accumulation rate. In order to calibrate Equation 3 to the

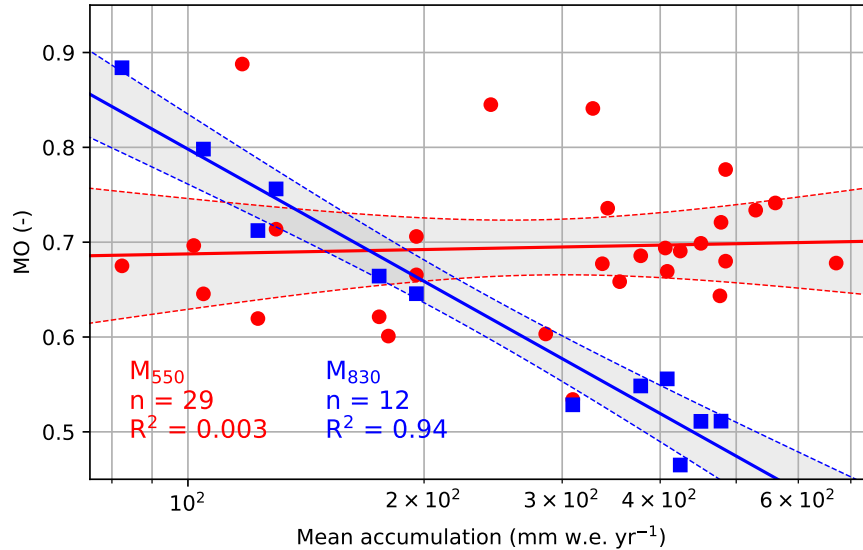


Figure 3. Ratio between modelled and observed depth at which the density reaches 550 kg m^{-3} (MO_{550}) or 830 kg m^{-3} (MO_{830}) as a function of local accumulation rate. The solid lines represent the corresponding regressions and the grey bands around them are their corresponding 95% confidence intervals.

140 new, expanded set of observations, we introduce a multiplication factor MO to better align modelled density profiles with observations:

$$MO = \alpha - \beta \ln(\dot{b}) \quad (4)$$

where α and β are unitless constants. In previous studies for the GrIS these were $\{\alpha, \beta\} = \{1.435, 0.151\}$ for $\rho < 550 \text{ kg m}^{-3}$ and $\{\alpha, \beta\} = \{2.366, 0.293\}$ for $\rho \geq 550 \text{ kg m}^{-3}$ (Kuipers Munneke et al. (2015a)). Although the physical processes underlying the densification of firm do not explicitly depend on the accumulation rate, a correlation between $\frac{d\rho}{dt}$ and \dot{b} may act as a proxy variable for effects that are time dependent, possibly related to the geometry of grains (Cuffey and Paterson (2011)). Firm densification owing to horizontal compression is neglected, although in fast-flowing regions this can be locally important (Horlings et al. (2021)).

In the model update, we recalibrated the dry densification correction factor MO as a function of mean annual accumulation, by using an updated, high-resolution GrIS accumulation field (Noël et al. (2015)) and optimizing the modelled depths at which the firm density reaches the critical values $550/830 \text{ kg m}^{-3}$ following Ligtenberg et al. (2011) and Kuipers Munneke et al. (2015a). To perform the previous calibration, we expanded the 22-core data set by Kuipers Munneke et al. (2015a) to 29 cores. Since MO corrects for the dry compaction rate, only dry firm cores (i.e. with little surface melt) are used. A core is considered as "dry" if the mean annual melt is less than 5% of the mean annual accumulation rate.. Least squares fitting yields R^2 values



Table 1. Values of the old and new linear regression of Eq. 4, their R^2 as well as the standard error in of the new fitting parameters.

	α_{old}	α_{new}	σ_α	β_{old}	β_{new}	σ_β	R_{old}^2	R_{new}^2
MO ₅₅₀	1.042	0.6569	0.1367	0.0916	-0.0067	0.0242	0.35	0.003
MO ₈₃₀	1.734	1.7243	0.0880	0.2039	0.2011	0.0161	0.96	0.940

155 for MO₅₅₀ and MO₈₃₀ of $2.82 \cdot 10^{-3}$ and 0.94 respectively. Fig. 3 shows the new calibrations and statistics of the new and old fit are summarised in Table 1.

With the update and the use of new firm and accumulation data, the linear relation between MO₅₅₀ and $\ln(\dot{b})$ vanishes, and reduces to an almost constant value of 0.7. Despite the difference with previous formulations in IMAU-FDM, this is similar to findings by Robin (1958) and Herron and Langway (1980), who also found that below 550 kg m^{-3} the densification rate correlates almost linearly with accumulation, and that this correlation became non-linear at higher densities. The high correlation for MO₈₃₀ also implies that the relation between densification rate $\frac{d\rho}{dt}$ and accumulation is non-linear above $\rho = 550 \text{ kg m}^{-3}$.

2.2.3 Thermal conductivity

In IMAU-FDM, the vertical temperature distribution and its evolution is obtained by solving the one-dimensional heat transfer equation

$$\rho c \frac{\partial T}{\partial t} = -\frac{\partial G}{\partial z} + \mathcal{L} = -\frac{\partial}{\partial z} \left(k \frac{\partial T}{\partial z} \right) + \mathcal{L} \quad (5)$$

in which c is the specific heat capacity of the firm, G the subsurface heat flux, k the thermal conductivity of the firm and \mathcal{L} a heat source representing the release of latent heat upon the refreezing of liquid water in the firm or the subsurface absorption of solar radiation. Subsurface penetration of short-wave radiation is neglected in the current model version, which is deemed a reasonable approximation for fine-grained, polar snow. The firm temperature profile is initialized using a spin-up period, see Sect. 2.2.6. Before the spin-up, the firm column is initialised at a constant temperature equal to the annual mean surface temperature during the spin-up period. The lower boundary condition assumes a constant heat flux across the lowest model grid cell, i.e. the deep temperature is allowed to change along with long-term changes in surface temperature or internal heat release. The upper boundary condition for the temperature calculation is provided by the surface ('skin') temperature in RACMO2, obtained by iteratively solving the surface energy balance (Van den Broeke et al. (2008)). Subsequently, for computational efficiency Eq. 5 is solved using an implicit/explicit scheme in the absence/presence of liquid water (Helsen et al. (2008)). Due to the Lagrangian character of the model, vertical heat advection is implicitly considered (Helsen et al. (2008)). Any heat generated by firm horizontal/vertical deformation is neglected.

The thermal conductivity is assumed to depend on firm density and temperature, and in previous versions of IMAU-FDM followed the expression for seasonal snow due to Anderson (1976), which only depends on density. In the updated model, the parameterization for thermal conductivity as a function of firm density of Calonne et al. (2019) is used. The new expression



more accurately models the dynamics of the thermal conductivity by incorporating both a density and temperature dependency. The new expression was obtained from 3D images of firn micro-structures at different temperatures, and is valid for the wide range of density and temperature values typically encountered in ice sheet firn layers, making it suitable for simulations of the
185 GrIS. It takes on the following form:

$$k(\rho, T) = (1 - \theta) \frac{k_i(T)k_a(T)}{k_i(-3^\circ\text{C})k_a(-3^\circ\text{C})} k_{snow}(\rho) + \theta \frac{k_i(T)}{k_i(-3^\circ\text{C})} k_{firn}(\rho) \quad (6)$$

The equation consists of two parts: one for snow and low-density firn and one for ice and high-density firn. The transition between the two regimes remains smooth through the weight factor $\theta(\rho)$. The definition of θ and the thermal conductivities that are used in Eq. 6 are:

190 $\theta = 1/(1 + \exp(-0.04(\rho - 450)))$

$$k_i(T) = 9.828 \exp(-0.0057T)$$

$$k_a(T) = (2.334 \cdot 10^{-3} T^{3/2}) / (164.54 + T)$$

$$k_{snow}(\rho) = 0.024 - 1.23 \cdot 10^{-4} \rho + 2.5 \cdot 10^{-6} \rho^2$$

$$k_{firn}(\rho) = 2.107 + 0.003618(\rho - \rho_i)$$

195 Here k_a represents the thermal conductivity of air, taken from Reid et al. (1959). Figure 4 compares the old and new expressions for various temperatures. As can be seen, the new expression takes on a slightly lower value than Anderson (1976) at densities below $\sim 475-565 \text{ kg m}^{-3}$, depending on the temperature, but a higher value at densities above that. This difference becomes larger at lower temperatures.

2.2.4 Meltwater percolation, retention and refreezing

200 IMAU-FDM employs a tipping bucket method to treat the percolation, irreducible (capillary) retention and (re)freezing of water, by filling up subsequent deeper layers to maximum capacity in a single model time step (i.e. quasi-instantaneous). Magnusson and others (Magnusson et al. (2015)) show that, in spite of its simplicity and shortcomings, the tipping bucket method is a robust and useful method to deal with liquid water transport in the snowpack when compared to more sophisticated methods, especially when capturing general firn properties at the larger, multi-kilometre horizontal scale for which IMAU-
205 FDM is designed. In IMAU-FDM, the fraction that is retained in a model layer by capillary forces ('irreducible water content') depends on the available pore space according to the expression by Coléou and Lesaffre (1998):

$$W_c = 1.7 + 5.7 \frac{P}{1 - P} \quad (7)$$

where P is the porosity of the firn layer, defined as $P = 1 - \rho/\rho_i$. The maximum amount of water that is stored thus decreases with increasing density of the firn layer. Standing water and lateral runoff over ice-layers are currently ignored; the latter is

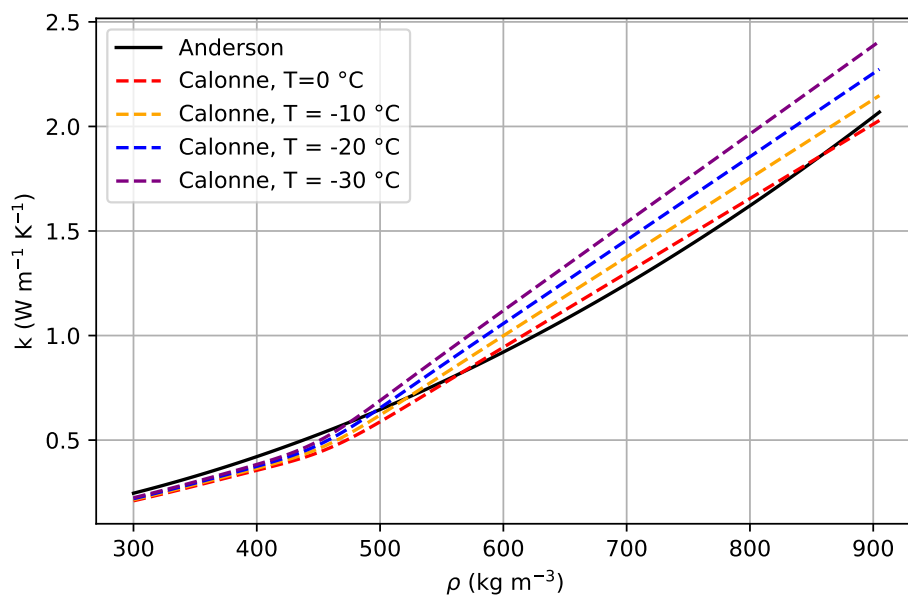


Figure 4. Comparison of the thermal conductivity parameterisation by Anderson (1976) and Calonne et al. (2019) with density at different temperatures.

210 considered a fair assumption, because on the spatial scales at which the model is employed (i.e. the RACMO2 grid of 5.5 by 5.5 km) it is assumed that within a model grid cell the meltwater can usually find a way to flow around a layer of ice. Varying the irreducible water content by, e.g., multiplying Eq. 7 with a constant factor or using a constant volume or mass fraction, did not improve the result, and it was decided to leave the liquid water scheme unchanged.

2.2.5 Firm thickness and elevation change

215 IMAU-FDM tracks the total firm thickness, and changes in it. The resulting vertical velocity of the ice-sheet surface due to changes in the firm layer ($\frac{dh}{dt}$) is given by:

$$\frac{dh}{dt} = v_{snow} + v_{snd} + v_{er} + v_{melt} + v_{ice} + v_{fc} \quad (8)$$

The total vertical surface velocity $\frac{dh}{dt}$ can thus be decomposed into separate contributions from accumulation (v_{snow}), surface sublimation (included in v_{snow}), sublimation by snowdrift (v_{snd}), erosion or deposition by snowdrift (v_{er}), snowmelt (v_{melt}), 220 and firm compaction (v_{fc}). The term v_{ice} is defined as the mean surface mass balance (SMB, $v_{ice} = v_{snow} + v_{snd} + v_{er} + v_{melt}$) with an opposite sign. It represents the long-term average vertical mass flux through the lower boundary of the firm column, which equals the mass flux through the upper boundary in a steady-state firm layer. In Sect. 4 we show surface elevation change and the individual components for three case study locations on the GrIS.



2.2.6 Model initialisation

225 The latest IMAU-FDM model runs span the period 1 January 1960 - 31 December 2020. The initial model density, temperature and liquid water content in the firn column are obtained by repeatedly applying the spin-up period 1960 - 1979 during which the forcing (i.e. surface accumulation, liquid water flux and temperature) is assumed to have remained reasonably constant (i.e. no significant long-term trends, Van den Broeke et al. (2009)). Observations and model studies support the assumption that the Greenland climate and SMB started to change significantly in the 1990s (Enderlin et al. (2014); McMillan et al. (2016)),
230 confirming that the period 1960 - 1979 can be selected for initialization purposes. Initialization is considered complete when the entire firn layer (up to the pore close-off density of 830 kg m^{-3}) has been refreshed. The required number of iterations depends on accumulation rate, and is typically 10 to 20 for the relatively dry grid points in the northeastern GrIS and typically 25 to 45 for the relatively wet southeastern GrIS. After the spin-up is finished, the model completes the run by once applying the 1980-2020 forcing from RACMO2.3p2.

235 2.3 RACMO2.3p2 forcing

At the upper boundary of IMAU-FDM, mass accumulation (solid precipitation minus sublimation minus drifting snow erosion), liquid water fluxes (melt plus rainfall minus evaporation) and surface temperature are prescribed from the regional atmospheric climate model RACMO2.3p2, which has been used to simulate the climate and surface mass balance of the GrIS and its immediate surroundings for the period 1958-2020 at a horizontal resolution of 5.5 km. This version of RACMO2
240 has been extensively evaluated over the GrIS (Noël et al. (2018b)). At the lateral boundaries, using a relaxation zone of 24 gridpoints, RACMO2 is forced by European Centre for Medium-Range Weather Forecasts (ECMWF) re-analysis data, i.e. ERA-40 between 1958 and 1978, ERA-Interim between 1979 and 1990 and ERA-5 between 1991 and 2020. For the forcing of IMAU-FDM the full spatial resolution of 5.5 km is used and a temporal resolution of 3 hours was selected, as an acceptable trade-off between robustly resolving the daily cycle and keeping manageable file sizes. IMAU-FDM typically uses a timestep
245 of 3 min (explicit temperature calculation scheme) to 3 h (implicit temperature calculation scheme), for which we linearly interpolate the forcing between the RACMO2 forcing time steps.

3 Model performance

3.1 Firn density

The vertical density profiles of 92 GrIS firn cores are used to assess the performance of the updated model. For each available
250 firn core, IMAU-FDM has been run at the grid point closest to that location. The evaluation is not completely independent of the calibration, as the 29 cores used for fitting the MO-values are also included. As an integrated measure of porosity, we

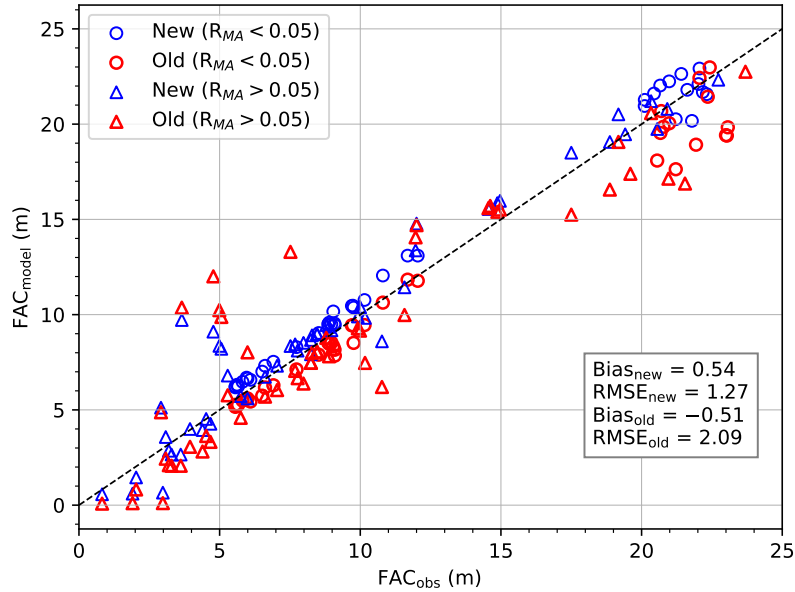


Figure 5. Modelled vs observed firm air content in metres. Dry locations are indicated with circles whereas wet locations are indicated with triangles.

compare modelled and observed vertically integrated firm air content (FAC), i.e. the vertical distance over which the firm layer can be compressed until reaching the density of glacier ice across the entire firm column.

$$\text{FAC} = \sum_j^{n_z} \frac{(\rho_i - \rho_j)}{\rho_i} \Delta z_j \quad (9)$$

255 Here, n_z is the number of layers in that firm profile, Δz_j is the thickness of layer j and ρ_j is the density of that layer. Note that here the FAC is calculated over the complete depth at which observations are available, as opposed to FAC_{10} shown in Fig. 1 which was calculated over the top 10 m. FAC is an indicator of the meltwater retention capacity of the firm layer and therewith an important parameter to simulate correctly. In general, one can state that locations on the GrIS with $\text{FAC} > 15$ m (Fig. 1) experience little to no melt, whereas the locations with $\text{FAC} < 15$ m do experience significant melt and refreezing,
 260 which uses up part of the pore space.

With the newly adopted parametrizations, the simulation of FAC in dry locations has significantly improved (Fig. 5). For these 39 locations, the root mean squared error (RMSE) decreased from 1.45 to 0.83 m (-43%). The improvement is more modest for low FAC locations, where the previous underestimation has now become a small overestimation. For these 53 locations, the RMSE decreased from 2.53 to 1.58 m (-38%). For all cores combined, the mean bias and RMSE have decreased
 265 from $-0.40/2.14$ to $0.61/1.32$ m respectively.

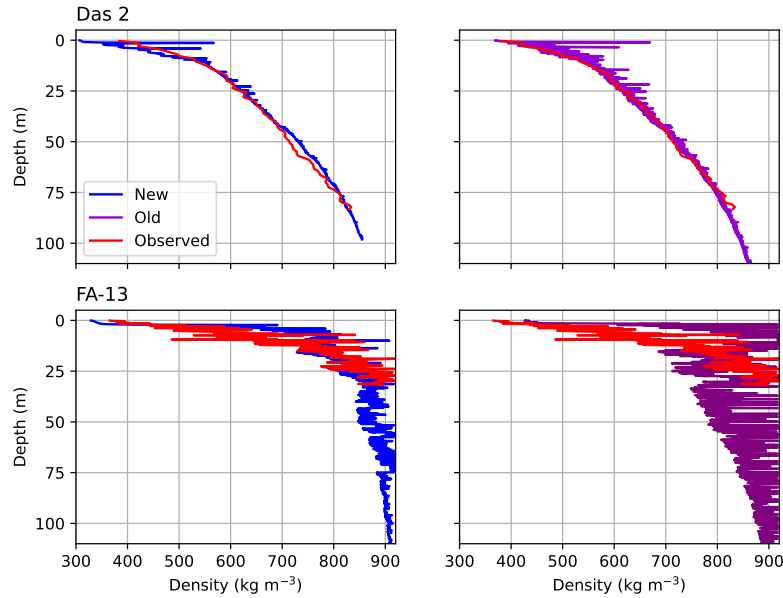


Figure 6. Density profiles for the new (left) and old (right) model settings at Das 2 (top) and FA-13 (bottom).

Fausto et al. (2018) noted that surface density correlates only weakly with annual mean T_a and that using a constant density of 315 kg m^{-3} may be considered. To assess this, we compared FAC for the old and the new model with and without temperature dependence. In order to identify possible depth-dependent biases we also define a cost function, Φ , to quantify the error in the modelled density profile:

$$270 \quad \Phi = \sqrt{\frac{1}{n_z} \sum_i^{n_z} (\rho_{model,i} - \rho_{obs,i})^2} \quad (10)$$

The RMSE in FAC decreased from 2.14 m with the old settings, to 1.32 m with the new settings, including a temperature dependent surface snow density and 1.44 m when using a constant surface snow density of 315 kg m^{-3} . Similarly, the mean Φ of all density profiles decreased from 50.3 kg m^{-3} to 44.4 and 41.0 kg m^{-3} respectively when using the new settings with and without temperature dependency for surface snow density. These results show that including temperature as a predictor for the surface density does improve model performance. Thus, we opt for the temperature dependent formulation, since this also allows capturing the effect of long-term temperature trends on the surface density.

Fig. 6 shows observed and modelled density profiles from the locations Das2 and FA-13, sites with large and small FAC respectively. Das2 is a dry location, with very little melt (4 mm w.e.yr^{-1}) and changes to its profile whereas FA-13 experiences strong melt ($406 \text{ mm w.e.yr}^{-1}$). At both sites, the new model settings improved the modelled density-depth profile, with a

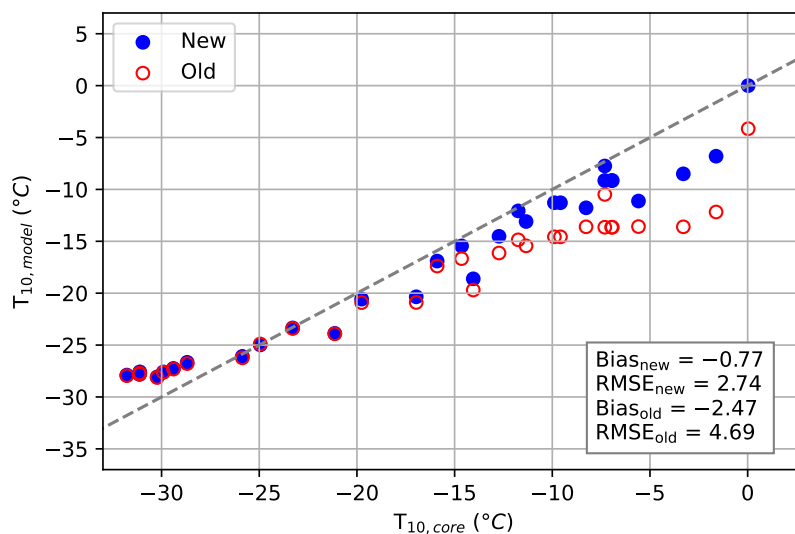


Figure 7. Modelled vs. observed temperature at 10 m depth (in °C) for 31 locations on the GrIS.

280 more realistic shape and reduced variability. It increases the pore space and brings simulated FAC in better agreement with the observed density profile. One of the main reason for the increased performance is the change from an instantaneous surface density parameterization to one that is based on annual mean values. This leads to greatly reduced "peaks" in the density profile, which is much more in line with observations since the surface density. For FA-13, it also seems that the lower surface density matches the upper 25 m of the density profile better.

285 3.2 Firn temperature

Modelled and measured 10 m firn temperatures at 31 locations are compared in Fig. 7. The new settings improve results, especially for the warmer locations with significant melt, which are mostly locations from Harper et al. (2012a) in west Greenland. Here, the cold bias has been significantly reduced; for locations with $T_{10} > -20$ °C, the mean RMSE decreased from 4.7 to 2.7 °C, respectively (-43%).

290 The main reason for the improvement is a better representation of the density at those locations, which allows for more realistic refreezing and the associated enhanced latent heat release, increasing the temperature in melt-prone locations. Additionally, the lower conductivity due to the lower density leads to a less efficient cooling of the deeper snow during winter. In spite of the clear improvement, a cold-bias remains for some of these locations, which can be partly attributed to a cold-bias in the RACMO2 forcing. For the low-melt locations ($T_{10} < -20$ °C), a persistent warm model bias remains.

295 Fig. 8 compares the observed temperature profiles of Summit and Dye-2 in winter and summer with the new and old model results. Similarly to what was found in Fig. 7, Summit, which is a dry and cold location has a warm bias whereas Dye-2, which

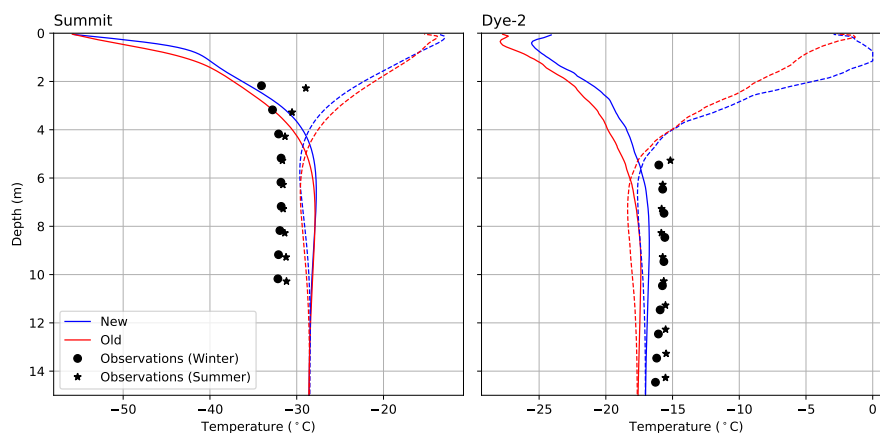


Figure 8. Comparison between observed temperature profiles vs. the new settings and the old model results in summer (dashed lines) and winter (solid lines) at Summit in winter (9 March 2002) and summer (6 August 2002) and Dye-2 in the summer (10 August 2007) and winter (13 March 2007).

is warm and wet, has a cold bias. For both locations the new surface density parameterization has decreased the density in the upper layers. This in turn leads to a lower thermal conductivity since the thermal conductivity increases monotonically with density (Fig. 4). Therefore, heat diffuses slower in the upper layers, increasing the temperature gradient there, which can be seen clearly at Summit. For both locations the depth at which the thermal maximum occurs also decreased slightly.

Dye-2 now clearly shows a temperature maximum at the depth at which refreezing occurs in contrast to the old model settings. This is also attributed to a decrease in the thermal conductivity: previously, heat generated by refreezing was able to more rapidly diffuse to greater depths or the atmosphere, but now it remains "trapped" around the depth at which refreezing occurs. Another factor that contributes is that refreezing occurs at a greater depth than before, see Sect. 3.3.

3.3 Liquid water content

The liquid water percolation and retention schemes have not been updated, but the changes made to the parameterizations that impact density and temperature do influence water percolation, and therewith liquid water content (LWC), and these changes are discussed here. Very few in-situ, vertically resolved observations of LWC are available. Here we used data from a recent study that used upward looking ground penetrating radar (upGPR) at Dye-2 in the higher percolation zone of the southwestern GrIS (2120 ma.s.l., see Fig. 1, Heilig et al. (2020)).

Fig. 9 compares the old and the new model results against the observed evolution of the maximum penetration depth and LWC in the firn. The measurements reveal that the melt in 2016 at Dye-2 mostly occurred in four periods between July and October, the timings of which are well captured in the RACMO2.3p2 forcing. Comparing old and new model settings, the water penetration depth and LWC have both increased. This mainly reflects the decreased density in the upper layer at Dye-2. As discussed in the previous section, this leads to an increase in the temperature in the upper firn layer and stronger temperature

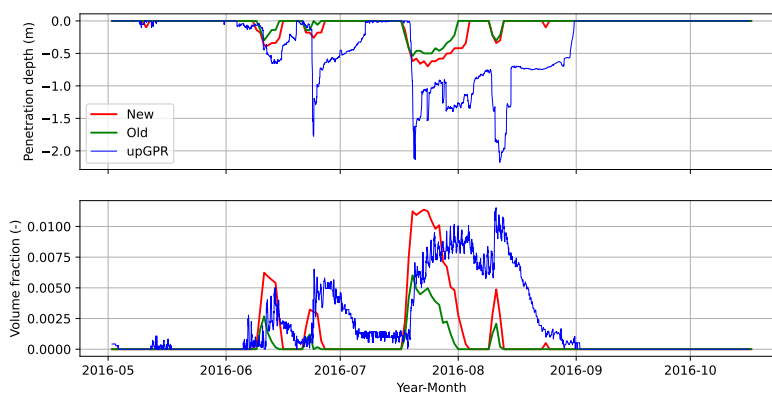


Figure 9. Comparison between the observed penetration depth (top) and volume fraction (bottom) of liquid water at Dye-2 with the new and old model results.

gradients at Dye-2. The increase in temperature means that the water needs to percolate deeper into the firn pack before it can refreeze, which is reflected in the increased penetration depth. Simultaneously, the decrease of the surface density means that there is more pore space near the surface that can retain irreducible water, explaining the increase in volume fraction. Overall, the penetration depth now agrees better with the observations, although in IMAU-FDM, the meltwater still refreezes
320 too quickly in more shallow layers than observed.

4 Pilot application to firn-induced surface elevation change

In this section we compare time series (1958-2020) of firn-induced surface elevation (i.e. firn depth) changes at three key locations: Summit in the cold and dry ice sheet interior, KAN-U in the relatively warm and dry southwestern percolation zone and FA-13 in the wet and relatively mild southeastern firn aquifer region (Koenig et al. (2014); Forster et al. (2014), as
325 indicated by the green circles in Fig. 1). Table 2 provides geographical and climatological information of these locations. The three locations represent three very different climates and are therefore useful for investigating how the new model settings affect firn depth change, which represents the surface elevation change in the absence of contributions from ice dynamics, basal melt and/or bedrock elevation change.

4.1 Summit

330 Summit is located at the centre of the GrIS at a high elevation and therefore it experiences a low amount of snowfall and a negligible amount of rain and melt. The evolution of its elevation is therefore closely linked to changes in the temperature (higher temperatures lead to a higher compaction rate) and accumulation (higher accumulation leads to a higher surface elevation).

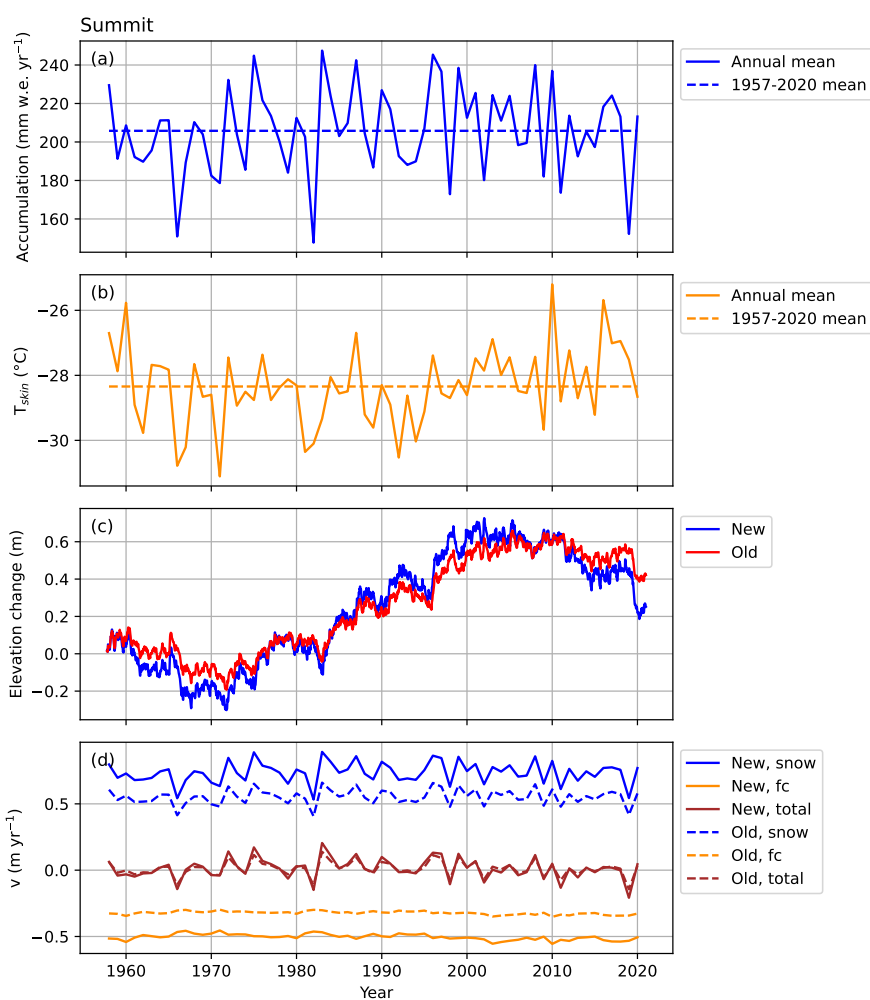


Figure 10. Time series of the total annual accumulation, the annual mean skin temperature, the height change and mean annual velocity components at Summit.



Table 2. Location and climate climate of the three case study sites. The annual mean accumulation are calculated over the whole simulation period (1957-2020).

	Lon. (°W)	Lat. (°N)	Elevation (m a.s.l.)	$T_{2\text{ m}}$ (°C)	Acc. (mm w.e.)	Melt (mm w.e.)
Summit	38.32	72.55	3281	-26.0	206	0
KAN-U	47.02	67.00	1840	-12.4	480	271
FA-13	39.04	66.18	1563	-7.0	986	496

Fig. 10 shows how annual accumulation and mean annual skin temperature change over the course of the simulation period, as well as changes to the surface elevation and its velocity components, both for the new and old model settings.

335 At Summit, an 0.8 m elevation change between 1970 and 2000 ($\sim 2.5 \text{ cm yr}^{-1}$) is modelled, with a slightly decreasing firn depth in the periods before and after. This can be explained by lower accumulation before about 1970 and after 2000, along with slightly increased temperatures since 2000. Differences in simulated surface elevation between old and new model settings are small. Nevertheless, the individual velocity components being very different.

As shown in the bottom panel of Fig. 10, the interannual variability in firn depth is dominated by snowfall (v_{snow}), which
 340 is compensated mainly by steady firn compaction (v_{fc}). From this it follows that the slightly higher accumulation and lower temperature between ~ 1970 and 2000 caused the net upward surface velocity. As a result, net vertical velocity reduces to almost zero, leading to a relatively stable surface elevation. Overall, the net vertical velocity of the surface is very similar between the old and the new versions. At the same time, both v_{snow} and v_{fc} have increased in magnitude almost equally. The new surface density parameterization (Eq. 1) leads to a lower surface density, which in turn is compensated for by a higher
 345 densification rate in order to match the observed set of z_{550} and z_{830} values. It is reflected by larger MO values: MO_{550} has increased from 0.56 to 0.69 and MO_{830} has increased from 0.62 to 0.66. Thus, with a lower surface density, the vertical upward velocity of the surface is higher, and the compaction velocity v_{fc} has also increase by an almost equal amount. This explains why overall total vertical velocity, and the resulting surface elevation change does not differ much between the old and new settings.

350 However, the new settings do result in larger seasonal and interseasonal oscillations in the firn depth. This is because v_{snow} and v_{fc} act on different timescales. v_{fc} is fairly constant in time and changes in tandem with the seasonal changes in temperature. v_{snow} on the other hand is much more variable, as snowfall is very episodic and highly variable at many time scales. As a result, the surface elevation increases more during a snowfall event and decreases during dry episodes, and these ratios have increased in the new model, leading to larger interannual variations. This also implies that the firn model is now more sensitive
 355 to changes in the forcing, reacting more strongly to a decrease or increase in accumulation and skin temperature in the future.

4.2 KAN-U

Situated in the southwest and at a lower elevation, KAN-U is warmer than Summit, but most importantly, melting occurs every year during the summer, which greatly affects the firn properties at its location (Fig. 11). The average influence of surface melt

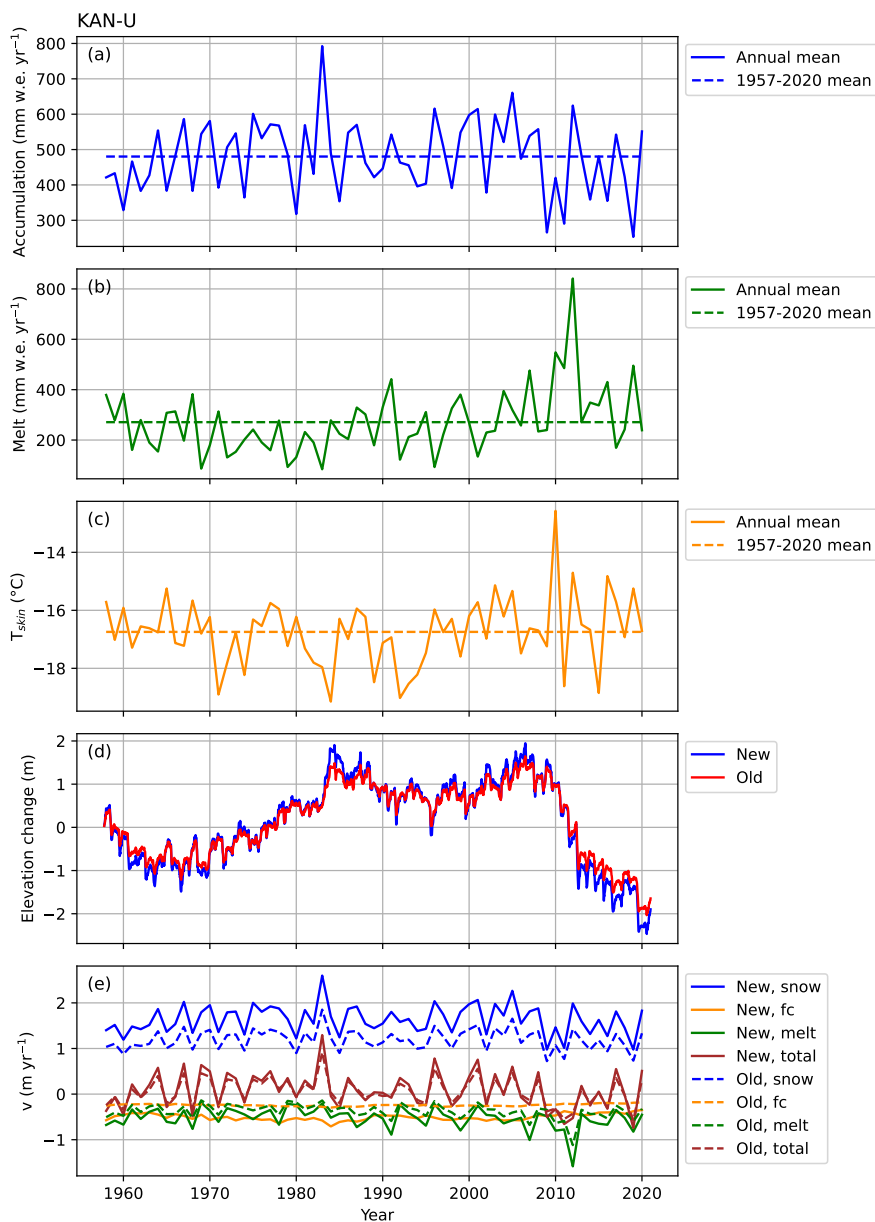


Figure 11. Time series of annual accumulation, melt, annual mean skin temperature, surface elevation change and mean annual vertical velocity components at KAN-U.



on firn depth changes (v_{melt}) is similar in magnitude and sign to the contribution from compaction (v_{fc}): it decreases the depth
360 of the firn column and decreases its air content.

At KAN-U, a 2.5 m thickening is modelled between 1970 and 1985. If we look at the associated climate forcing, this can be explained by a relatively low amount of melt and a low temperature during this period. Between 2005 and 2020, a rapid decline (-20 cm yr^{-1}) is observed, which is associated with a strong increase in surface melt since 2005, as well as a slight increase in temperature and a reduction in the number of high-accumulation years. The most striking changes in elevation at KAN-U
365 occurred in exceptional years, like 1983 as a very wet year, 2010 as a very warm year, and 2012 as an extremely high-melt year.

When comparing the vertical surface velocities between the old and the new model settings, we again see an increased accumulation velocity v_{snow} , due to a lower fresh snow density. This is again compensated for by a more negative compaction velocity, resulting in a very similar net velocity (v_{tot}). As accumulation decreased after 2005, the net effect on the surface
370 is a slight lowering. Following significant warming and increased melt at this site (Fig. 11), the contribution of v_{melt} to firn depth changes increases and that of v_{fc} decreases, making the former the dominant process leading to surface lowering at KAN-U. The strong increase in melt causes a larger downward velocity of the surface, leading to thinning. v_{melt} is also larger in magnitude with the new settings because the melted snow at the surface is of a lower density.

Just like at Summit, the elevation change is more sensitive to its forcing with the new model settings than previously was the
375 case. This is especially apparent in the years 1983 and 2012. Throughout the time series, interannual variability in firn depth is first dominated by snowfall (v_{snow}), but towards the end of the time series the contribution to the total variability made by v_{melt} increases rapidly.

4.3 FA-13

At the two previous sites the new model settings produce similar results for the overall surface elevation change. However,
380 at the third site of FA-13, a site with a firn aquifer, we found that the new model settings produce a significantly different result compared to the old ones. This location experiences a warmer and wetter climate than KAN-U, which leads to a rapid densification in the upper part of the firn column (Fig. 6).

Here, the signal is dominated by large seasonal oscillations in firn depth of up to $\sim 1 \text{ m yr}^{-1}$ between 1960 and 1985. From 1985 onwards, the firn depth decreases until 2012, but at a higher rate in the updated than in the previous model (~ 0.35 vs.
385 0.25) m yr^{-1} throughout the time series.

For the vertical velocity components, a similar picture emerges at FA-13 as at KAN-U, where a significant melt increase means that v_{melt} becomes the dominant source of elevation lowering since 2005. The contribution of melt to surface elevation changes becomes more important throughout the simulation period, because the melt itself increases and becomes more variable, and also because the variability in accumulation decreases over time. At FA-13 the new model settings show the same
390 signature in the individual vertical-velocity components as at the other two sites: accumulation leads to more surface thickening due to the lower fresh-snow density. To compensate, compaction also increases. The compaction in the new model set-up is stronger and shows more interannual variability, in line with the larger interannual variability of the annual accumulation.

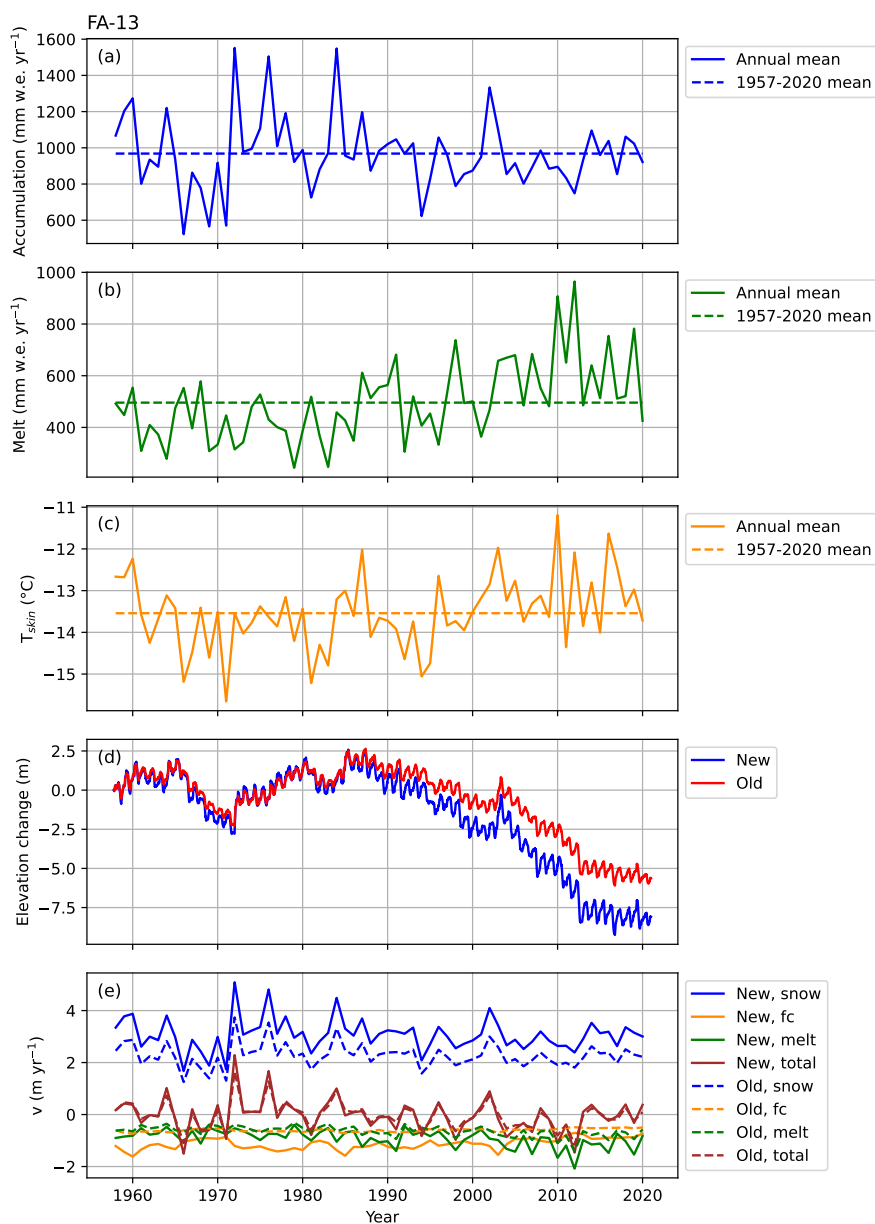


Figure 12. Time series of annual accumulation, melt, annual mean skin temperature, surface elevation change and mean annual vertical velocity components at FA-13.



Vertical surface velocity due to surface melt is very different in the new model version compared to the old one. Both the variability and the magnitude of the melt is stronger in the new model. In the period 1990-2020, 8.5 m of thinning occurred in
395 the new model, compared to 6 m in the old model. Since the uppermost layers of snow are structurally less dense in the new model, surface melt implies a stronger lowering of the surface for less dense snow, as demonstrated in Fig 11 and 12. It is clear that the new model has larger downward surface velocity than the old model especially in strong melt years. It corroborates the idea that strong melt events over less dense snow lead to stronger surface lowering.

5 Summary and outlook

400 Temporal and spatial variability in firn thickness is highly relevant for the mass balance of the Greenland ice sheet (GrIS), because it directly impacts its refreezing efficiency. Moreover, firn thickness change is an important component of surface elevation change, and improved knowledge is required to accurately convert remotely sensed GrIS volume to mass changes. In this paper, we presented improvements in the offline version of the IMAU firn densification model (IMAU-FDM v1.2G), forced by three-hourly output of the regional climate model RACMO2.3p2. Taking advantage of improved climate forcing
405 and newly available observations of surface and subsurface firn density and temperature, the improvements are systematically implemented in the parametrizations of surface density, dry snow densification and thermal conductivity. The treatment of liquid water is not changed, owing to a lack of sufficient observations to justify changes in the current configuration.

The updated model predicts predicts higher firn air content (FAC), which at three selected sites in the interior GrIS and in the southwestern and southeastern percolation zone results in a larger sensitivity of firn thickness to intra- and interannual
410 variations in snowfall, melt and temperature. As an important consequence of a change in fresh snow density parameterization, the inter- and intra-annual variations in elevation have increased, owing to an increased sensitivity to changes in its forcing. In a warmer climate, firn thinning owing to increased surface melt becomes increasingly important at the marginal sites, both in the mean and as a component of interannual variability. Future applications of the improved model include a full GrIS assessment of contemporary and future firn mass and thickness changes, as well as explaining areas where firn aquifers and ice slabs
415 currently occur, and their future changes.

Code availability. The code of IMAU-FDM v1.2G used in this project is available on GitHub at <https://github.com/brils001/IMAU-FDM> and at Zenodo (<https://zenodo.org/record/5172513>, Brils et al. (2021)).

Author contributions. MB, PKM, WJvdB and MRvdB started this project, decided on its scope, which parts of the model required further development and interpreted the results. MB performed the model simulations, implemented the changes to the model, comparisons and led
420 the writing of the manuscript. All authors contributed to discussions on the manuscript.



Competing interests. The authors declare that they have no conflict of interest.

Acknowledgements. This work was carried out under the program of the Netherlands Earth System Science Centre (NESSC), financially supported by the Ministry of Education, Culture and Science (OCW grant no. 024.002.001). We acknowledge ECMWF for computational time on their supercomputers.



425 References

- Anderson, E. E. a.: A point energy and mass balance model of a snow cover, vol. 114, <http://www.csa.com/partners/viewrecord.php?requester=gs{%&}collection=ENV{%&}recid=7611864{%}%}5Cnhttp://www.agu.org/pubs/crossref/2009/2009JD011949.shtml>, 1976.
- Arthern, R. J., Vaughan, D. G., Rankin, A. M., Mulvaney, R., and Thomas, E. R.: In situ measurements of Antarctic snow compaction compared with predictions of models, *Journal of Geophysical Research: Earth Surface*, 115, 1–12, <https://doi.org/10.1029/2009JF001306>,
430 2010.
- Banta, J. R. and McConnell, J. R.: Annual accumulation over recent centuries at four sites in central Greenland, *Journal of Geophysical Research Atmospheres*, 112, 1–9, <https://doi.org/10.1029/2006JD007887>, 2007.
- Box, J. E., Cressie, N., Bromwich, D. H., Jung, J. H., Van den Broeke, M., Van Angelen, J. H., Forster, R. R., Miège, C., Mosley-Thompson, E., Vinther, B., and McConnell, J. R.: Greenland ice sheet mass balance reconstruction. Part I: Net snow accumulation (1600–2009), *Journal of Climate*, 26, 3919–3934, <https://doi.org/10.1175/JCLI-D-12-00373.1>, 2013.
435
- Brils, M., Kuipers Munneke, P., Van de Berg, W. J., and Van den Broeke, M.: IMAU-FDM v1 GDM release, <https://doi.org/10.5281/ZENODO.5172513>, 2021.
- Calonne, N., Milliancourt, L., Burr, A., Philip, A., Martin, C. L., Flin, F., and Geindreau, C.: Thermal Conductivity of Snow, Firn, and Porous Ice From 3-D Image-Based Computations, *Geophysical Research Letters*, 46, 13 079–13 089, <https://doi.org/10.1029/2019GL085228>,
440 2019.
- Charalampidis, C., Van As, D., Box, J. E., Van den Broeke, M. R., Colgan, W. T., Doyle, S. H., Hubbard, A. L., MacFerrin, M., Machguth, H., and P. Smeets, C. J.: Changing surface-atmosphere energy exchange and refreezing capacity of the lower accumulation area, West Greenland, *Cryosphere*, 9, 2163–2181, <https://doi.org/10.5194/tc-9-2163-2015>, 2015.
- Coléou, C. and Lesaffre, B.: Irreducible water saturation in snow: experimental results in a cold laboratory, *Annals of Glaciology*, 26, 64–68,
445 <https://doi.org/10.3189/1998aog26-1-64-68>, 1998.
- Cuffey, K. and Paterson, W.: The physics of glaciers, *Journal of Glaciology*, 57, 383–384, https://www.cambridge.org/core/product/identifier/S0022143000206242/type/journal{%}_article, 2011.
- Enderlin, E. M., Howat, I. M., Jeong, S., Noh, M.-J., Van Angelen, J. H., and van den Broeke, M. R.: An improved mass budget for the Greenland ice sheet, *Geophysical Prospecting*, pp. 6413–6419, <https://doi.org/10.1002/2014GL061184>. Received, 2014.
- 450 Fausto, R. S., Box, J. E., Vandecrux, B., van As, D., Steffen, K., MacFerrin, M. J., Machguth, H., Colgan, W., Koenig, L. S., McGrath, D., Charalampidis, C., and Braithwaite, R. J.: A snow density dataset for improving surface boundary conditions in Greenland ice sheet firn modeling, *Frontiers in Earth Science*, 6, <https://doi.org/10.3389/feart.2018.00051>, 2018.
- Forster, R. R., Box, J. E., Van den Broeke, M. R., Miège, C., Burgess, E. W., Van Angelen, J. H., Lenaerts, J. T., Koenig, L. S., Paden, J., Lewis, C., Gogineni, S. P., Leuschen, C., and McConnell, J. R.: Extensive liquid meltwater storage in firn within the Greenland ice sheet,
455 *Nature Geoscience*, 7, 95–98, <https://doi.org/10.1038/ngeo2043>, 2014.
- Hanna, E., McConnell, J., Das, S., Cappelen, J., and Stephens, A.: Observed and modeled Greenland Ice Sheet snow accumulation, 1958–2003, and links with regional climate forcing, *Journal of Climate*, 19, 344–358, <https://doi.org/10.1175/JCLI3615.1>, 2006.
- Harper, J., Humphrey, N., Pfeffer, W. T., Brown, J., and Fettweis, X.: Greenland ice-sheet contribution to sea-level rise buffered by meltwater storage in firn - supplementary material, *Nature*, 491, 240–243, <https://doi.org/10.1038/nature11566>, 2012a.
- 460 Harper, J., Humphrey, N., Pfeffer, W. T., Brown, J., and Fettweis, X.: Greenland ice-sheet contribution to sea-level rise buffered by meltwater storage in firn, *Nature*, 491, 240–243, <https://doi.org/10.1038/nature11566>, 2012b.



- Heilig, A., Eisen, O., MacFerrin, M., Tedesco, M., and Fettweis, X.: Seasonal monitoring of melt and accumulation within the deep percolation zone of the Greenland Ice Sheet and comparison with simulations of regional climate modeling, *Cryosphere*, 12, 1851–1866, <https://doi.org/10.5194/tc-12-1851-2018>, 2018.
- 465 Heilig, A., Eisen, O., Schneebeli, M., MacFerrin, M., Stevens, C. M., Vandecrux, B., and Steffen, K.: Relating regional and point measurements of accumulation in southwest Greenland, *The Cryosphere*, 14, 385–402, <https://doi.org/10.5194/tc-14-385-2020>, 2020.
- Helsen, M. M., Van den Broeke, M. R., Van De Wal, R. S., Van De Berg, W. J., Van Meijgaard, E., Davis, C. H., Li, Y., and Goodwin, I.: Elevation changes in antarctica mainly determined by accumulation variability, *Science*, 320, 1626–1629, <https://doi.org/10.1126/science.1153894>, 2008.
- 470 Herron, M. M. and Langway, C. C.: Firn densification: an empirical model., *Journal of Glaciology*, 25, 373–385, <https://doi.org/10.1017/S0022143000015239>, 1980.
- Horlings, A. N., Christianson, K., Holschuh, N., Stevens, C. M., and Waddington, E. D.: Effect of horizontal divergence on estimates of firn-air content, *Journal of Glaciology*, 67, 287–296, <https://doi.org/10.1017/jog.2020.105>, 2021.
- Keenan, E., Wever, N., Dattler, M., Lenaerts, J. T., Medley, B., Kuipers Munneke, P., and Reijmer, C.: Physics-based SNOWPACK model improves representation of near-surface Antarctic snow and firn density, *Cryosphere*, 15, 1065–1085, <https://doi.org/10.5194/tc-15-1065-2021>, 2021.
- Koenig, L. and Montgomery, L.: Surface mass balance and snow depth on sea ice working group (SUMup) snow density subdataset, Greenland and Antarctica, 1950–2018, <https://doi.org/10.18739/A26D5PB2S>, 2019.
- Koenig, L., Box, J., and Kurtz, N.: Improving surface mass balance over ice sheets and snow depth on sea ice, *Eos*, 94, 100, <https://doi.org/10.1002/2013EO100006>, 2013.
- 480 Koenig, L. S., Miège, C., Forster, R. R., and Brucker, L.: Initial in situ measurements of perennial meltwater storage in the Greenland firn aquifer, *Geophysical Research Letters*, 41, 81–85, <https://doi.org/10.1002/2013GL058083>, 2014.
- Kuipers Munneke, P., Ligtenberg, S. R., Noël, B. P., Howat, I. M., Box, J. E., Mosley-Thompson, E., McConnell, J. R., Steffen, K., Harper, J. T., Das, S. B., and Van den Broeke, M. R.: Elevation change of the Greenland Ice Sheet due to surface mass balance and firn processes, 1960–2014, *Cryosphere*, 9, 2009–2025, <https://doi.org/10.5194/tc-9-2009-2015>, 2015a.
- 485 Kuipers Munneke, P., Ligtenberg, S. R., Suder, E. A., and Van den Broeke, M. R.: A model study of the response of dry and wet firn to climate change, *Annals of Glaciology*, 56, 1–8, <https://doi.org/10.3189/2015AoG70A994>, 2015b.
- Ligtenberg, S. R., Helsen, M. M., and Van den Broeke, M. R.: An improved semi-empirical model for the densification of Antarctic firn, *Cryosphere*, 5, 809–819, <https://doi.org/10.5194/tc-5-809-2011>, 2011.
- 490 Ligtenberg, S. R., Munneke, P. K., Noël, B. P., and Van den Broeke, M. R.: Brief communication: Improved simulation of the present-day Greenland firn layer (1960–2016), *Cryosphere*, 12, 1643–1649, <https://doi.org/10.5194/tc-12-1643-2018>, 2018.
- Lundin, J. M., Stevens, C. M., Arthern, R., Buizert, C., Orsi, A., Ligtenberg, S. R., Simonsen, S. B., Cummings, E., Essery, R., Leahy, W., Harris, P., Helsen, M. M., and Waddington, E. D.: Firn Model Intercomparison Experiment (FirnMICE), *Journal of Glaciology*, 63, 401–422, <https://doi.org/10.1017/jog.2016.114>, 2017.
- 495 MacFerrin, M., Machguth, H., van As, D., Charalampidis, C., Stevens, C. M., Heilig, A., Vandecrux, B., Langen, P. L., Mottram, R., Fettweis, X., den Broeke, M. R., Pfeffer, W. T., Moussavi, M. S., and Abdalati, W.: Rapid expansion of Greenland’s low-permeability ice slabs, *Nature*, 573, 403–407, <https://doi.org/10.1038/s41586-019-1550-3>, 2019.



- Machguth, H., MacFerrin, M., Van As, D., Box, J. E., Charalampidis, C., Colgan, W., Fausto, R. S., Meijer, H. A. J., Mosley-Thompson, E., and van de Wal, R. S. W.: Greenland meltwater storage in firn limited by near-surface ice formation, *Nature Climate Change*, 6, 390–393, <https://doi.org/10.1038/nclimate2899>, 2016.
- Magnusson, J., Wever, N., Essery, R., Helbig, N., Winstral, A., and Jonas, T.: Evaluating snow models with varying process representations for hydrological applications, *Water Resources Research*, 51, 2707–2723, <https://doi.org/10.1002/2014WR016498>, 2015.
- McConnell, J. R., Mosley-Thompson, E., Bromwich, D. H., Bales, R. C., and Kyne, J. D.: Interannual variations of snow accumulation on the Greenland Ice Sheet (1985–1996): New observations versus model predictions, *Journal of Geophysical Research Atmospheres*, 105, 4039–4046, <https://doi.org/10.1029/1999JD901049>, 2000.
- McMillan, M., Leeson, A., Shepherd, A., Briggs, K., Armitage, T. W., Hogg, A., Kuipers Munneke, P., van den Broeke, M., Noël, B., van de Berg, W. J., Ligtenberg, S., Horwath, M., Groh, A., Muir, A., and Gilbert, L.: A high-resolution record of Greenland mass balance, *Geophysical Research Letters*, 43, 7002–7010, <https://doi.org/10.1002/2016GL069666>, 2016.
- Mosley-Thompson, E., McConnell, J. R., Bales, R. C., Li, Z., Lin, P. N., Steffen, K., Thompson, L. G., Edwards, R., and Bathke, D.: Local to regional-scale variability of annual net accumulation on the Greenland ice sheet from PARCA cores, *Journal of Geophysical Research Atmospheres*, 106, 33 839–33 851, <https://doi.org/10.1029/2001JD900067>, 2001.
- Mouginot, J., Rignot, E., Björk, A. A., van den Broeke, M., Millan, R., Morlighem, M., Noël, B., Scheuchl, B., and Wood, M.: Forty-six years of Greenland Ice Sheet mass balance from 1972 to 2018, *Proceedings of the National Academy of Sciences of the United States of America*, 116, 9239–9244, <https://doi.org/10.1073/pnas.1904242116>, 2019.
- Nghiem, S. V., Hall, D. K., Mote, T. L., Tedesco, M., Albert, M. R., Keegan, K., Shuman, C. A., DiGirolamo, N. E., and Neumann, G.: The extreme melt across the Greenland ice sheet in 2012, *Geophysical Research Letters*, 39, 6–11, <https://doi.org/10.1029/2012GL053611>, 2012.
- Noël, B., Van De Berg, W. J., Van Meijgaard, E., Kuipers Munneke, P., Van De Wal, R. S., and Van den Broeke, M. R.: Evaluation of the updated regional climate model RACMO2.3: Summer snowfall impact on the Greenland Ice Sheet, *Cryosphere*, 9, 1831–1844, <https://doi.org/10.5194/tc-9-1831-2015>, 2015.
- Noël, B., van de Berg, W. J., Lhermitte, S., Wouters, B., Machguth, H., Howat, I., Citterio, M., Moholdt, G., Lenaerts, J. T. M., and van den Broeke, M. R.: A tipping point in refreezing accelerates mass loss of Greenland’s glaciers and ice caps, *Nature Communications*, 8, 14 730, <https://doi.org/10.1038/ncomms14730>, 2017.
- Noël, B., van de Berg, W. J., Lhermitte, S., Wouters, B., Schaffer, N., and van den Broeke, M. R.: Six Decades of Glacial Mass Loss in the Canadian Arctic Archipelago, *Journal of Geophysical Research: Earth Surface*, 123, 1430–1449, <https://doi.org/10.1029/2017JF004304>, 2018a.
- Noël, B., van de Berg, W. J., van Wessem, J. M., van Meijgaard, E., van As, D., Lenaerts, J. T. M., Lhermitte, S., Kuipers Munneke, P., Smeets, C. J. P. P., van Ulft, L. H., van de Wal, R. S. W., and van den Broeke, M. R.: Modelling the climate and surface mass balance of polar ice sheets using RACMO2 – Part 1: Greenland (1958–2016), *The Cryosphere*, 12, 811–831, <https://doi.org/10.5194/tc-12-811-2018>, 2018b.
- Noël, B., van de Berg, W. J., Lhermitte, S., and van den Broeke, M. R.: Rapid ablation zone expansion amplifies north Greenland mass loss, *Science Advances*, 5, 2–11, <https://doi.org/10.1126/sciadv.aaw0123>, 2019.
- Noël, B., Jakobs, C. L., van Pelt, W. J., Lhermitte, S., Wouters, B., Kohler, J., Hagen, J. O., Luks, B., Reijmer, C. H., van de Berg, W. J., and van den Broeke, M. R.: Low elevation of Svalbard glaciers drives high mass loss variability, *Nature Communications*, 11, 1–8, <https://doi.org/10.1038/s41467-020-18356-1>, 2020.



- Orsi, A. J., Kawamura, K., Masson-Delmotte, V., Fettweis, X., Box, J. E., Dahl-Jensen, D., Clow, G. D., Landais, A., and Severinghaus, J. P.: The recent warming trend in North Greenland, *Geophysical Research Letters*, 44, 6235–6243, <https://doi.org/10.1002/2016GL072212>, 2017.
- Polashenski, C., Courville, Z., Benson, C., Wagner, A., Chen, J., Wong, G., Hawley, R., and Hall, D.: Observations of pronounced Greenland ice sheet firn warming and implications for runoff production, *Geophysical Research Letters*, 41, 4238–4246, <https://doi.org/10.1002/2014GL059806>, 2014.
- Reid, R. C., Sherwood, T. K., and Street, R. E.: The Properties of Gases and Liquids, *Physics Today*, 12, 38–40, <https://doi.org/10.1063/1.3060771>, 1959.
- Robin, G. D. Q.: Seismic shooting and related investigations: Norwegian-British-Swedish Antarctic Expedition, 1949–1952, *Scientific Results*, 5, [https://doi.org/10.1038/s43247-020-0010-1](https://scholar.google.com/scholar?hl=en&as{ }sdt=0{ }% }2C5{ }& }q=Robin+1958.+Glaciology.+Ill.+Seismic+shooting+and+related+investigations{ }& }btnG=, 1958.</p><p>Sasgen, I., Wouters, B., Gardner, A. S., King, M. D., Tedesco, M., Landerer, F. W., Dahle, C., Save, H., and Fettweis, X.: Return to rapid ice loss in Greenland and record loss in 2019 detected by the GRACE-FO satellites, <i>Communications Earth & Environment</i>, 1, <a href=), 2020.
- Shepherd, A., Ivins, E., Rignot, E., Smith, B., van den Broeke, M., Velicogna, I., Whitehouse, P., Briggs, K., Joughin, I., Krinner, G., Nowicki, S., Payne, T., Scambos, T., Schlegel, N., A. G., Agosta, C., Ahlström, A., Babonis, G., Barletta, V. R., Bjørk, A. A., Blazquez, A., Bonin, J., Colgan, W., Csatho, B., Cullather, R., Engdahl, M. E., Felikson, D., Fettweis, X., Forsberg, R., Hogg, A. E., Gallee, H., Gardner, A., Gilbert, L., Gourmelen, N., Groh, A., Gunter, B., Hanna, E., Harig, C., Helm, V., Horvath, A., Horvath, M., Khan, S., Kjeldsen, K. K., Konrad, H., Langen, P. L., Lecavalier, B., Loomis, B., Luthcke, S., McMillan, M., Melini, D., Mernild, S., Mohajerani, Y., Moore, P., Mottram, R., Mouginit, J., Moyano, G., Muir, A., Nagler, T., Nield, G., Nilsson, J., Noël, B., Ootosaka, I., Pattle, M. E., Peltier, W. R., Pie, N., Rietbroek, R., Rott, H., Sandberg Sørensen, L., Sasgen, I., Save, H., Scheuchl, B., Schrama, E., Schröder, L., Seo, K. W., Simonsen, S. B., Slater, T., Spada, G., Sutterley, T., Talpe, M., Tarasov, L., van de Berg, W. J., van der Wal, W., van Wessem, M., Vishwakarma, B. D., Wiese, D., Wilton, D., Wagner, T., Wouters, B., and Wuite, J.: Mass balance of the Greenland Ice Sheet from 1992 to 2018, *Nature*, 579, 233–239, <https://doi.org/10.1038/s41586-019-1855-2>, 2020.
- Steger, C. R., Reijmer, C. H., and Van den Broeke, M. R.: The modelled liquid water balance of the Greenland Ice Sheet, *Cryosphere*, 11, 2507–2526, <https://doi.org/10.5194/tc-11-2507-2017>, 2017a.
- Steger, C. R., Reijmer, C. H., van den Broeke, M. R., Wever, N., Forster, R. R., Koenig, L. S., Munneke, P. K., Lehning, M., Lhermitte, S., Ligtenberg, S. R., Miège, C., and Noël, B. P.: Firn meltwater retention on the greenland ice sheet: A model comparison, *Frontiers in Earth Science*, 5, <https://doi.org/10.3389/feart.2017.00003>, 2017b.
- Stevens, C. M., Verjans, V., Lundin, J., Kahle, E., Horlings, A., Horlings, B., and Waddington, E.: The Community Firn Model (CFM) v1.0, *Geoscientific Model Development Discussions*, pp. 1–37, <https://doi.org/10.5194/gmd-2019-361>, 2020.
- Van Dalum, C. T., Jan Van De Berg, W., Lhermitte, S., and Van den Broeke, M. R.: Evaluation of a new snow albedo scheme for the greenland ice sheet in the regional atmospheric climate model (racmo2), *Cryosphere*, 14, 3645–3662, <https://doi.org/10.5194/tc-14-3645-2020>, 2020.
- Van den Broeke, M., Smeets, P., Ettema, J., van der Veen, C., van De Wal, R., and Oerlemans, J.: Partitioning of melt energy and meltwater fluxes in the ablation zone of the west Greenland ice sheet, *Cryosphere*, 2, 179–189, <https://doi.org/10.5194/tc-2-179-2008>, 2008.
- Van den Broeke, M., Bamber, J., Ettema, J., Rignot, E., Schrama, E., Van Berg, W. J. D., Van Meijgaard, E., Velicogna, I., and Wouters, B.: Partitioning recent Greenland mass loss, *Science*, 326, 984–986, <https://doi.org/10.1126/science.1178176>, 2009.



- Van den Broeke, M. R., Enderlin, E. M., Howat, I. M., Kuipers Munneke, P., Noël, B. P., Jan Van De Berg, W., Van Meijgaard, E., and Wouters, B.: On the recent contribution of the Greenland ice sheet to sea level change, *Cryosphere*, 10, 1933–1946, <https://doi.org/10.5194/tc-10-1933-2016>, 2016.
- 575 Van Wessem, J. M., Steger, C. R., Wever, N., and Van den Broeke, M. R.: An exploratory modelling study of perennial firn aquifers in the Antarctic Peninsula for the period 1979–2016, *Cryosphere*, 15, 695–714, <https://doi.org/10.5194/tc-15-695-2021>, 2021.
- Vandecrux, B., Fausto, R., Van As, D., Colgan, W., Langen, P., Sampson, K., Steffen, K., Haubner, K., Ingemann-Nielsen, T., Niwano, M., and Box, J.: Heat budget of Greenland firn: observed and simulated changes from 1998–2015, *Tech. rep.*, 2019a.
- 580 Vandecrux, B., MacFerrin, M., MacHguth, H., Colgan, W. T., Van As, D., Heilig, A., Max Stevens, C., Charalampidis, C., Fausto, R. S., Morris, E. M., Mosley-Thompson, E., Koenig, L., Montgomery, L. N., Miège, C., Simonsen, S. B., Ingeman-Nielsen, T., and Box, J. E.: Firn data compilation reveals widespread decrease of firn air content in western Greenland, *Cryosphere*, 13, 845–859, <https://doi.org/10.5194/tc-13-845-2019>, 2019b.
- Vandecrux, B., Mottram, R., Langen, P. L., Fausto, R. S., Olesen, M., Stevens, M., Verjans, V., Leeson, A., Ligtenberg, S., Munneke, P. K., 585 Marchenko, S., Pelt, W. V., Meyer, C., Hewitt, I., Simonsen, S. B., Samimi, S., Machguth, H., Macferrin, M., and Niwano, M.: The firn meltwater Retention Model Intercomparison Project (RetMIP): Evaluation of nine firn models at four weather station sites on the Greenland ice sheet, <https://doi.org/10.5194/tc-2019-331>, 2020.
- Wouters, B., Martin-Español, A., Helm, V., Flament, T., Van Wessem, J. M., Ligtenberg, S. R., Van den Broeke, M. R., and Bamber, J. L.: Dynamic thinning of glaciers on the Southern Antarctic Peninsula, *Science*, 348, 899–903, <https://doi.org/10.1126/science.aaa5727>, 2015.
- 590 Zwally, H. J., Li, J., Robbins, J. W., Saba, J. L., Yi, D., and Brenner, A. C.: Mass gains of the Antarctic ice sheet exceed losses, *Journal of Glaciology*, 61, 1019–1036, <https://doi.org/10.3189/2015JoG15J071>, 2015.